Journal of Zhejiang University-SCIENCE C (Computers & Electronics)
ISSN 1869-1951 (Print); ISSN 1869-196X (Online)
www.zju.edu.cn/jzus; www.springerlink.com
E-mail: jzus@zju.edu.cn

Diffusion tensor interpolation profile control using non-uniform motion on a Riemannian geodesic*

Chang-Il SON[1,2], Shun-ren XIA[†‡1]

([1]*MOE Key Laboratory of Biomedical Engineering, Zhejiang University, Hangzhou 310027, China*)

([2]*Department of Electronics, Kim Chaek University of Technology, Pyongyang 104919, DPR of Korea*)

[†]E-mail: srxia@zju.edu.cn

Received Apr. 17, 2011; Revision accepted June 23, 2011; Crosschecked Dec. 29, 2011

Abstract: Tensor interpolation is a key step in the processing algorithms of diffusion tensor imaging (DTI), such as registration and tractography. The diffusion tensor (DT) in biological tissues is assumed to be positive definite. However, the tensor interpolations in most clinical applications have used a Euclidian scheme that does not take this assumption into account. Several Riemannian schemes were developed to overcome this limitation. Although each of the Riemannian schemes uses different metrics, they all result in a 'fixed' interpolation profile that cannot adapt to a variety of diffusion patterns in biological tissues. In this paper, we propose a DT interpolation scheme to control the interpolation profile, and explore its feasibility in clinical applications. The profile controllability comes from the non-uniform motion of interpolation on the Riemannian geodesic. The interpolation experiment with medical DTI data shows that the profile control improves the interpolation quality by assessing the reconstruction errors with the determinant error, Euclidean norm, and Riemannian norm.

Key words: Diffusion tensor (DT), DT imaging (DTI), DT interpolation, Interpolation profile control, Riemannian geodesic
doi:10.1631/jzus.C1100098 **Document code:** A **CLC number:** TP391.41

1 Introduction

Diffusion tensor imaging (DTI), as a modality of magnetic resonance imaging (MRI), is the unique water diffusion imaging technique for reconstructing white matter organization in the brain (Basser *et al.*, 1994; Filley, 2001; Schonberg *et al.*, 2006; Hoptman *et al.*, 2008; Roosendaal *et al.*, 2009). The registration (Alexander *et al.*, 2001; Zhang *et al.*, 2006) and tractography (Jones *et al.*, 1999; Snook *et al.*, 2007; Zhou *et al.*, 2008) of DTI plays an important role in clinical applications, and they all require tensor interpolation. Simple interpolation, based on Euclidean geometry, has been used in clinical applications recently (Pajevic and Basser, 2003; Peng *et al.*, 2009). However, this interpolation does not take into account the important properties of diffusion physics such as positive definiteness and invariance, which are guaranteed by a monotonic interpolation profile (Kindlmann *et al.*, 2007). Thus, some Riemannian schemes with different metrics, including the affine invariant metric (Batchelor *et al.*, 2005; Pennec *et al.*, 2006), Log-Euclidean metric (Arsigny *et al.*, 2006), and Riemannian symmetric space metric (Fletcher and Sarang, 2007), were proposed for tensor operation. Although the Riemannian schemes use different metrics, they all result in a 'fixed' interpolation profile that cannot adapt to a variety of diffusion patterns in biological tissues. The term 'interpolation profile' in this context indicates the generalization of interpolation curve (1D), surface (2D), and hyper-surface (larger than 3D) based on the same mathematical concept across space dimensionality. For example, we will use only the term 'linear profile', instead of two terms 'linear curve' and 'linear surface', for the interpolation of two tensors and the diffusion tensor (DT) image, respectively, in this context.

‡ Corresponding author

* Project (No. 60772092) supported by the National Natural Science Foundation of China

There are two ways to assess the interpolation quality. The first is to use the qualitative constraints, including the positive definiteness (Batchelor *et al.*, 2005) and the invariance of the clinical indices, such as the tensor determinant (Arsigny *et al.*, 2006; Pennec *et al.*, 2006; Fletcher and Sarang, 2007), trace, and fractional anisotropy (FA) (Kindlmann *et al.*, 2007). The second is to use the quantitative indices, such as the distance and determinant difference between the original DT image and the interpolated DT image (Arsigny *et al.*, 2006).

In this paper, we propose a Riemannian interpolation scheme to control the interpolation profile with respect to the tensor determinant. This scheme preserves the positive definiteness and determinant invariance. The control of the interpolation profile depends on the non-uniform motion on the Riemannian geodesic. Then the previous Riemannian interpolation schemes belong to the uniform motion class.

2 Theory and methodology

2.1 DT interpolation schemes

The diffusion tensor is represented as a 3×3 positive definite matrix $\boldsymbol{D}=(d_{ij})$, $i, j\in\{1, 2, 3\}$. First, let us consider several interpolation schemes for two tensors $\boldsymbol{D}_1$ at time 0 and $\boldsymbol{D}_2$ at time 1.

1. Euclidean linear interpolation. A tensor $\boldsymbol{D}$ is mapped to a six-dimensional vector $\boldsymbol{v}=(d_{11}, d_{22}, d_{33}, d_{12}, d_{13}, d_{23})$, and the tensor interpolated at time $t\in[0, 1]$ is computed as

$$\boldsymbol{v}(t)=(1-t)\boldsymbol{v}_1+t\boldsymbol{v}_2,\quad t\in[0,\ 1].$$

The Euclidian distance between two tensors $\boldsymbol{D}_1$ and $\boldsymbol{D}_2$ is given by

$$\mathrm{dist}(\boldsymbol{D}_1,\boldsymbol{D}_2)=\sqrt{\mathrm{tr}\,(\boldsymbol{D}_1-\boldsymbol{D}_2)^2}.$$

2. Riemannian symmetric space scheme (RSS) (Fletcher and Sarang, 2007). A geodesic $\boldsymbol{\gamma}_{\mathrm{RSS}}(t)$ from tensor $\boldsymbol{D}_1=\boldsymbol{\gamma}(0)$ to tensor $\boldsymbol{D}_2=\boldsymbol{\gamma}(1)$ defines the interpolated tensor $\boldsymbol{D}(t)$ at time $t\in[0, 1]$:

$$\boldsymbol{\gamma}_{\mathrm{RSS}}(t)=\boldsymbol{D}(t)=(\boldsymbol{g}\boldsymbol{v})\exp(t\boldsymbol{\Sigma})(\boldsymbol{g}\boldsymbol{v})^{\mathrm{T}},$$

where $\boldsymbol{g}$, $\boldsymbol{v}$, and $\boldsymbol{\Sigma}$ are Lie-group action symmetric matrices derived from $\boldsymbol{D}_1$ and $\boldsymbol{D}_2$. For details, see Fletcher and Sarang (2007).

The Riemannian distance between two tensors is written as

$$\mathrm{dist}(\boldsymbol{D}_1,\boldsymbol{D}_2)=\sqrt{\mathrm{tr}\,(\log\boldsymbol{\Sigma})^2}.$$

3. Log-Euclidean scheme (LE) (Arsigny *et al.*, 2006). The geodesic $\boldsymbol{\gamma}_{\mathrm{LE}}(t)$ is a computationally efficient close approximation of the Riemannian scheme:

$$\boldsymbol{\gamma}_{\mathrm{LE}}(t)=\exp[(1-t)\log\boldsymbol{D}_1+t\log\boldsymbol{D}_2]. \qquad (1)$$

The LE distance between two tensors is computed by

$$\mathrm{dist}(\boldsymbol{D}_1,\boldsymbol{D}_2)=\sqrt{\mathrm{tr}\,(\log\boldsymbol{D}_1-\log\boldsymbol{D}_2)^2}.$$

Fig. 1 shows the interpolation results in $t\in[0, 1]$ for two synthetic tensors $\boldsymbol{D}_1=\boldsymbol{\gamma}(0)$ and $\boldsymbol{D}_2=\boldsymbol{\gamma}(1)$ using different schemes. Here the synthetic tensors were produced as in Alexander and Barker (2005). The diffusion ellipsoids $\boldsymbol{\gamma}(t)$ with t=0.2, 0.4, 0.6, 0.8 interpolated by the Euclidian scheme are larger than those at the same time points interpolated by the two Riemannian schemes (Fig. 1a). In the interpolation curves of the tensor determinant (Fig. 1b), the interpolation profiles of LE and RSS schemes are monotonic and entirely the same. That is to say, the different Riemannian schemes always result in a

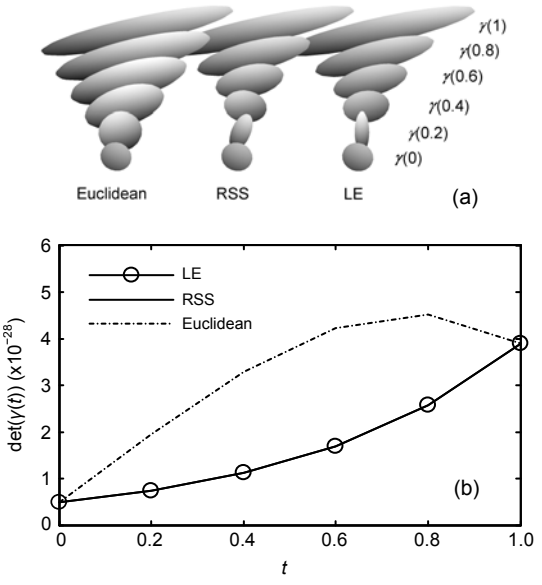

Fig. 1 The diffusion ellipsoids of interpolated tensors (a) and the interpolation curves of the tensor determinant (b) using Euclidian, RSS, and LE schemes

'fixed' interpolation profile of the tensor determinant. On the other hand, the interpolation curve from the Euclidean scheme is non-monotonic (Fig. 1b), resulting in the swelling effect (Chefd'Hotel *et al.*, 2004): a part of interpolated tensors have larger determinants than both of the two original tensors $\boldsymbol{D}_1$ and $\boldsymbol{D}_2$, which violates the diffusion physics in biological tissues.

2.2 Interpolation profile control

In mathematical interpolation between two scalars, we can select various interpolation profiles such as linear, spline, or polynomial expression. Unfortunately, in the tensor interpolation using Riemannian schemes, there was only one unique profile of power function $\det \boldsymbol{D}(t)=a^{1-t}b^t$, where $a=\det \boldsymbol{D}_1$, $b=\det \boldsymbol{D}_2$ (Fig. 1 and Eq. (3)). Therefore, the schemes could not adapt to a variety of diffusion patterns in biological tissues. In this subsection we explore an alternative scheme. In this scheme, the fixed interpolation profile is exchanged with an arbitrary monotonic profile. Since Riemannian schemes have the same interpolation curves, i.e., $\det(\boldsymbol{\gamma}_{\mathrm{RSS}}(t))\equiv\det(\boldsymbol{\gamma}_{\mathrm{LE}}(t))$, we refer both of them to an expression $\det(\boldsymbol{\gamma}_{\mathrm{Ri}}(t))$.

When normalizing the length of a Riemannian geodesic between two tensors as a unit, the tensor set on the geodesic can be written as $\boldsymbol{\gamma}(s)$, $s\in[0, 1]$. Let us consider the Riemannian interpolation kinetically.

Definition 1 (Riemannian based kinetic tensor interpolation) Provided that the interpolation moves from the start point $s=0$ to the end point $s=1$ on the geodesic, let the velocity be $v(t)=\dfrac{\mathrm{d}f(t)}{\mathrm{d}t}$. The interpolation after any time $t\in[0, 1]$ arrives at $f(t)=\int_0^t v(t)\mathrm{d}u$. The one-to-one mapping relation $\boldsymbol{\gamma}(s=f(t))$ between the time space (i.e., interpolation space) $t\in[0, 1]$ and the tensor set $\boldsymbol{\gamma}(s)$, $s\in[0, 1]$ is called 'Riemannian based kinetic tensor interpolation' (simply, 'Riemannian tensor interpolation' or 'tensor interpolation' below).

Definition 2 (Uniform velocity and non-uniform velocity interpolations) If $v(t)$ is constant, the tensor interpolation is called a 'uniform velocity interpolation'; if $v(t)$ is not constant, the tensor interpolation is a 'non-uniform velocity interpolation'.

First, note that the previous interpolations using the Riemannian scheme can be regarded as the interpolation with uniform velocity $v(t)=1$, so that $f(t)=t$. If the interpolation adopts non-uniform velocity $v(t)=\dfrac{\mathrm{d}f(t)}{\mathrm{d}t}$, $f(0)=0$, $f(1)=1$, $t\in[0, 1]$, the original Riemannian interpolation geodesic $\boldsymbol{\gamma}_{\mathrm{Ri}}(t)$ is rewritten as $\boldsymbol{\gamma}_{\mathrm{Ri}}(f(t))$. Then the interpolation profile of tensor determinant $\det(\boldsymbol{\gamma}_{\mathrm{Ri}}(t))$ is deformed to $\det(\boldsymbol{\gamma}_{\mathrm{Ri}}(f(t)))$. Although the interpolation profile is deformed, the positive definiteness and monotonic property of tensor interpolation are preserved as long as the interpolation moves along the geodesic with a positive velocity. Then the original interpolation $\boldsymbol{\gamma}_{\mathrm{Ri}}(t)$ belongs to the linear control class with $f(t)=t$.

Next, consider how to control the interpolation profile to fit an arbitrary profile. This problem is defined to find a mapping

$$f: t\to u,\ \psi(t)=\det(\boldsymbol{\gamma}_{\mathrm{Ri}}(u)),\ t,u\in[0, 1], \tag{2}$$

where $\boldsymbol{\gamma}_{\mathrm{Ri}}(u)$ is the Riemannian interpolation geodesic, $\det(\boldsymbol{\gamma}_{\mathrm{Ri}}(u))$ is the Riemannian interpolation profile between two tensor determinants, and $\psi(t)$ is a required interpolation profile such as the spline curve. We can obtain the following expression from Eq. (1) using the properties of logarithm, exponential operation, and symmetry of the tensor (Fletcher and Sarang, 2007):

$$\begin{gathered}\det(\boldsymbol{\gamma}_{Ri}(u))=\det(\boldsymbol{D}_1^{1-u}\cdot\boldsymbol{D}_2^{u})=a^{1-u}b^{u},\\ a=\det\boldsymbol{D}_1,\ b=\det\boldsymbol{D}_2.\end{gathered} \tag{3}$$

Consequently, the relationship between t and u is derived from Eqs. (2) and (3):

$$u=f(t)=\frac{\log(\psi(t)/a)}{\log(b/a)}. \tag{4}$$

And the DT interpolation $\boldsymbol{\gamma}(t)$ with profile $\psi(t)$ is given as follows:

$$\boldsymbol{\gamma}(t)=\boldsymbol{\gamma}_{\mathrm{Ri}}(f(t)),\ \mathrm{Ri}\in\{\mathrm{LE}, \mathrm{RSS}\}. \tag{5}$$

Although the permutation (4) is derived from LE scheme (1), this interpolation profile control (5) can be used for all the Riemannian interpolations, since the interpolation profiles of the tensor determinant are all the same.

The relationships $f(t)$ for several interpolation profiles are presented below:

1. Riemannian profile (Eq. (3)):

$$\psi(t)=\det(\boldsymbol{\gamma}_{\mathrm{Ri}}(t))=a^{1-t}b^{t}\text{, so } f(t)=t.$$

2. Linear profile:

$$\psi(t)=(b-a)t+a,$$

and then

$$f(t)=\frac{\log[1+t(b-a)/a]}{\log(b/a)}.$$

3. Harmonic profile:

If $a<b$, then

$$\psi(t)=[\sin(\pi t-\pi/2)+1](b-a)/2+a,$$

and

$$f(t)=\frac{\log\{1+[\sin(\pi t-\pi/2)+1](b-a)/(2a)\}}{\log(b/a)}.$$

If $a\geq b$, then

$$\psi(t)=[\cos(\pi t-\pi)+1](b-a)/2+a,$$

and

$$f(t)=\frac{\log\{1+[\cos(\pi t-\pi)+1](b-a)/(2a)\}}{\log(b/a)}.$$

Fig. 2 shows the example of Riemannian, linear, and harmonic profiles (Fig. 2a) and the interpolated DT ellipsoids (Fig. 2b) between two prolate tensors with the same direction and different diffusion volumes. The diffusion ellipsoid series (Fig. 2b) interpolated under the three interpolation profiles illustrates the evident differences at the corresponding time points. The diffusion ellipsoids under the Riemannian profile are always smaller than the ellipsoids under the other two profiles. The first half (about $\boldsymbol{\gamma}(0)$–$\boldsymbol{\gamma}(0.5)$) of the ellipsoids under the linear profile are larger than these under the harmonic profile, while the ramaining are smaller. This illustrates that the interpolation is controlled correctly according to the required profile.

2.3 Profile control in the two-dimensional space

For four neighboring diffusion tensors $\boldsymbol{D}_i$ (i=1, 2, 3, 4) at image grids in the 2D DT image space (x, y), the coordinates are denoted as $\boldsymbol{p}_i=(u_i, v_i)$, $u_i, v_i\in\{0, 1\}$, $i\in$1, 2, 3, 4 and the tensor determinants are A_i, i=1, 2, 3, 4. In the LE scheme, a 2D Riemannian geodesic surface $\boldsymbol{\gamma}_{\mathrm{Ri}}(x, y)$ is expressed as the positive weighted

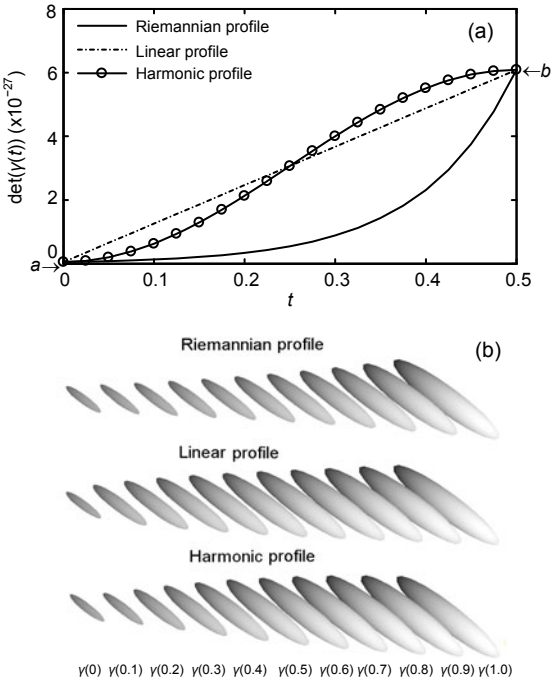

Fig. 2 Different interpolation profiles in our proposed scheme (a) and interpolated diffusion tensor ellipsoids (b)

sum of the logarithm of four tensors (Arsigny *et al.*, 2006):

$$\boldsymbol{\gamma}_{\mathrm{Ri}}(x,y)=\exp\left(\sum_{i=1}^{4}w_i(x,y)\log\boldsymbol{D}_i\right), \tag{6}$$

where

$$w_i(x,y)=[(1-u_i)+(-1)^{1-u_i}x][(1-v_i)+(-1)^{1-v_i}y].$$

Then the interpolation profile control problem is defined to find the map

$$f:\ (x,y)\rightarrow(\eta,\xi),\ \ \psi(x,y)=\det(\boldsymbol{\gamma}_{\mathrm{Ri}}(\eta,\xi)),$$

where $\psi(x, y)$ is the required interpolation profile, $\det(\boldsymbol{\gamma}_{\mathrm{Ri}}(\eta,\xi))=\prod_{i=1}^{4}A_i^{w_i(\eta,\xi)}$ (refer to Eq. (3)).

Compared to the interpolation of two tensors (Section 2.2), the determinant $\det(\boldsymbol{\gamma}_{\mathrm{Ri}}(\eta, \xi))$, which fits to $\psi(x, y)$, is not unique and forms a level-set $\Omega=\{\boldsymbol{\gamma}_{\mathrm{Ri}}(\eta, \xi)|\det(\boldsymbol{\gamma}_{\mathrm{Ri}}(\eta, \xi))=\psi(x, y)\}$. Therefore, we can determine the interpolation uniquely by finding the $\boldsymbol{\gamma}_{\mathrm{Ri}}(\eta, \xi)\in\Omega$ with the minimum Riemannian distance from $\boldsymbol{\gamma}_{\mathrm{Ri}}(x, y)$.

The unique interpolation $\boldsymbol{\gamma}_{\mathrm{Ri}}(\eta, \xi)$ is obtained as follows. First, Eq. (6) is used to calculate $\boldsymbol{\gamma}_{\mathrm{Ri}}(x, y)$, and then Eq. (7) is used to derive the four candidates $\boldsymbol{\gamma}_k$, k=1, 2, 3, 4 on the geodesics from $\boldsymbol{\gamma}_{\mathrm{Ri}}(x, y)$ to four

tensors $\boldsymbol{D}_k$, k=1, 2, 3, 4, respectively.

$$u_k = \frac{\log(\psi(x,y)/a)}{\log(A_k/a)},\ \ a = \det(\boldsymbol{\gamma}_{\mathrm{Ri}}(x,y)),\ k = 1,2,3,4, \tag{7}$$

$$\boldsymbol{\gamma}_k = \exp[(1-u_k)\log(\boldsymbol{\gamma}_{\mathrm{Ri}}(x,y)) + u_k \log \boldsymbol{D}_k]. \tag{8}$$

Finally the unique interpolation is determined as

$$\boldsymbol{\gamma}(x,y) = \underset{k}{\operatorname{argmin}}(\operatorname{dist}(\boldsymbol{\gamma}_{\mathrm{Ri}}(x,y),\ \boldsymbol{\gamma}_k)), \tag{9}$$

where dist(·,·) is a Riemannian distance function. Here the LE distance is used.

Fig. 3 illustrates the interpolation results using the RSS scheme, the LE scheme, the interpolation using linear profile $\psi(x,y) = \sum_{i=1}^{4} w_i(x,y)A_i$, and the Euclidean scheme. Here, all figures in the left column are the interpolation profiles of the tensor determinant and all figures in the right column are the DT ellipsoid images interpolated by the profile. The Riemannian schemes of RSS and LE have the same interpolation profile of the DT determinant while the interpolated DT ellipsoid patterns are a bit different. In fact, the anisotropy in the LE scheme increases a little more than that in the RSS scheme, but it is difficult to distinguish the difference with the naked eye, as mentioned in Arsigny *et al.* (2006).

Compared with the linear profile scheme, Riemannian schemes have a larger gap between DT ellipsoids due to the smaller diffusion ellipsoids than in the linear profile case, and the interpolation profile border of Riemannian schemes exhibits the power function pattern. In the linear profile scheme, the interpolation profile border is linear. The Euclidean interpolation profile illustrates the evident swelling effect. A part of the interpolation profile surface is higher than the four corner tensor determinants.

The extension of this interpolation scheme to 3D is straightforward by exchanging $\boldsymbol{\gamma}_{\mathrm{Ri}}(x,y)$, $\psi(x,y)$, and corner number 4 with $\boldsymbol{\gamma}_{\mathrm{Ri}}(x,y,z)$, $\psi(x,y,z)$, and corner number 8.

3 Experiments and results

3.1 Materials

The DTI dataset was acquired using a dual spin-echo, single shot echo-planar imaging sequence on a Siemens Sonata 1.5 T scanner. The acquisition parameters were 3-mm slice thickness, no inter-slice gap, TR (repeat time)=8100 ms, TE (echo time)= 92 ms, FOV=240 mm×240 mm, and four averages. Twelve non-collinear diffusion-sensitizing gradient directions with diffusion sensitivity b=1000 s/mm^2 and one non-diffusion-sensitizing gradient b=0 s/mm^2 were adopted. Fifty contiguous axial slices were acquired and each slice image is 128×128 pixels. The 12 gradient directions were as follows: [(1.0, 0.0, 0.5), (0.0, 0.5, 1.0), (0.5, 1.0, 0.0), (1.0, 0.5, 0.0), (0.0, 1.0, 0.5), (0.5, 0.0, 1.0), (1.0, 0.0, −0.5), (0.0, −0.5, 1.0), (−0.5, 1.0, 0.0), (1.0, −0.5, 0.0), (0.0, 1.0, −0.5), (−0.5, 0.0, 1.0)].

3.2 Method

With the medical DTI data, we used the four schemes of Euclidean, RSS, LE, and the proposed (linear profile) interpolations to reconstruct a DTI slice downsampled by a factor of 2. One of two columns and one of two rows were removed using the downsampling. This reconstruction is the interpolation at t=0.5 so that the linear profile and harmonic profile of the proposed scheme result in the same reconstruction (Fig. 2a). Therefore, we selected the linear profile for the computational simplicity. The slice was chosen in the mid-axial plane where strong variations are present in the DT image. After reconstruction, we produced the absolute value image of the pixel-wise difference tensor between the original and interpolated DT images for reconstruction error analysis. The absolute value tensor was defined as the symmetric positive semi-definite matrix obtained by replacing the eigenvalues of the original tensor with their absolute values. This absolute value image of DT retains all the information about the magnitude and the orientation (Arsigny *et al.*, 2006).

Then for quantitative comparison, we assessed the reconstruction errors with three error measures (see the Appendix): determinant, Euclidean norm, and Riemannian norm on the absolute value image. The error measures were computed as the total sum of pixel-wise errors on the selected slices. Since the diffusion tensor is a coefficient matrix of the Stejskal-Tanner equation (Stejskal and Tanner, 1965) for water molecule diffusion, it has no unit. Accordingly, the associated measures also have no unit. The smaller error measure reflects the better reconstruction result.

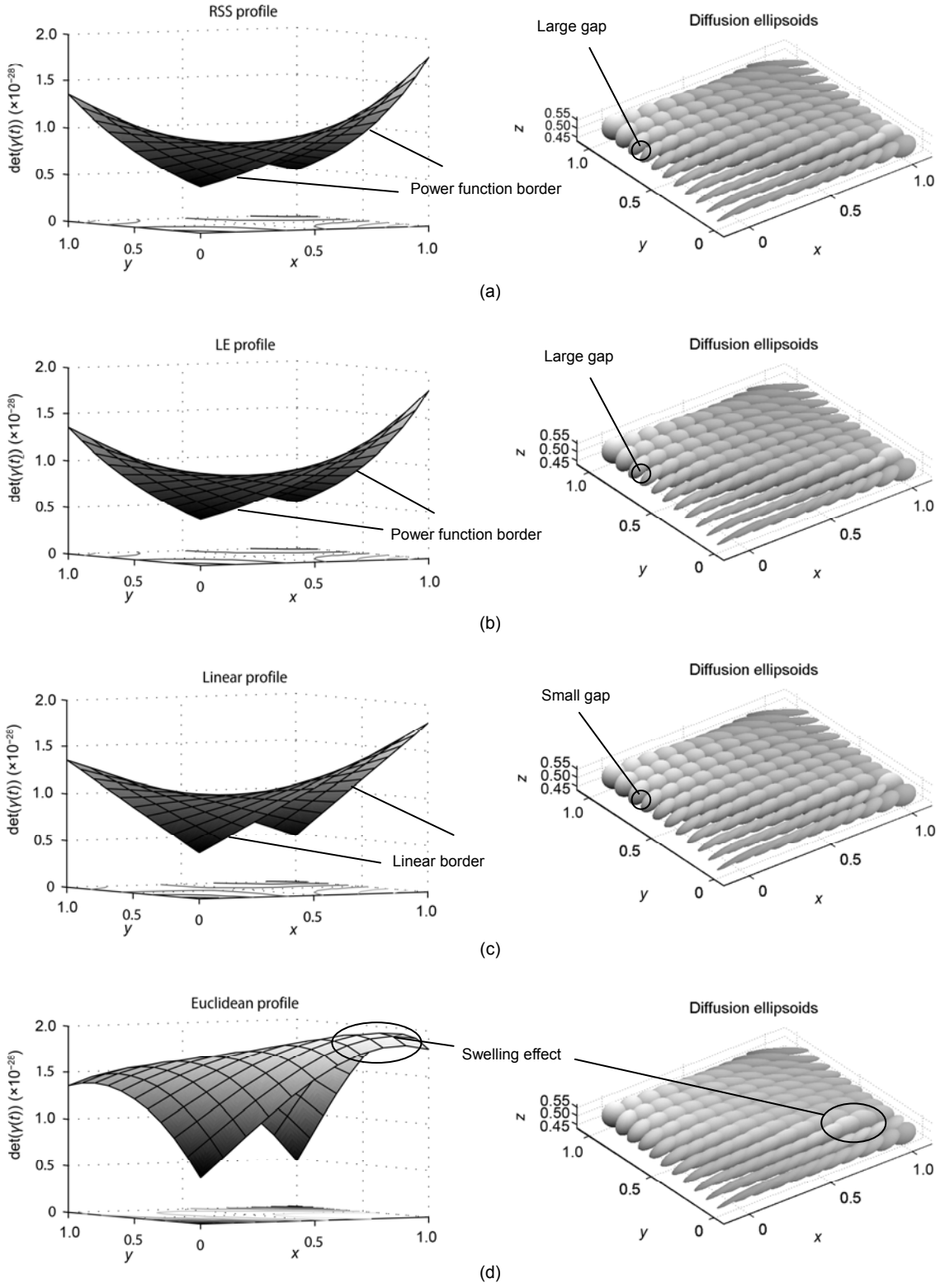

Fig. 3 The two-dimensional diffusion tensor (DT) interpolation: (a) RSS interpolation; (b) LE interpolation; (c) interpolation using a linear profile; (d) Euclidian interpolation

In each interpolation, the left figure is the interpolation profile of the tensor determinant and the right figure is the DT ellipsoid

3.3 Results

3.3.1 Absolute value image

Fig. 4 displays the absolute value image by using reconstruction error ellipsoids of the diffusion tensor. Fig. 4a shows the FA image of the middle axial slice and Fig. 4b illustrates the original diffusion tensor ellipsoids within the rectangle part of the FA image. The rectangle range is a typical part with different diffusion patterns and large reconstruction error ellipsoids. The large isotropic tensors occur in the ventricle, anisotropic tensors in the corpus callosum, and oblate tensors in the other part. The absolute value images for the four interpolation schemes are illustrated in Figs. 4c–4f. Here the larger ellipsoid represents the larger reconstruction error.

3.3.2 Reconstruction error

Table 1 provides the quantitative comparison between the four interpolation schemes by using three error measures: determinant error, Euclidean norm, and Riemannian norm. For the determinant error, the

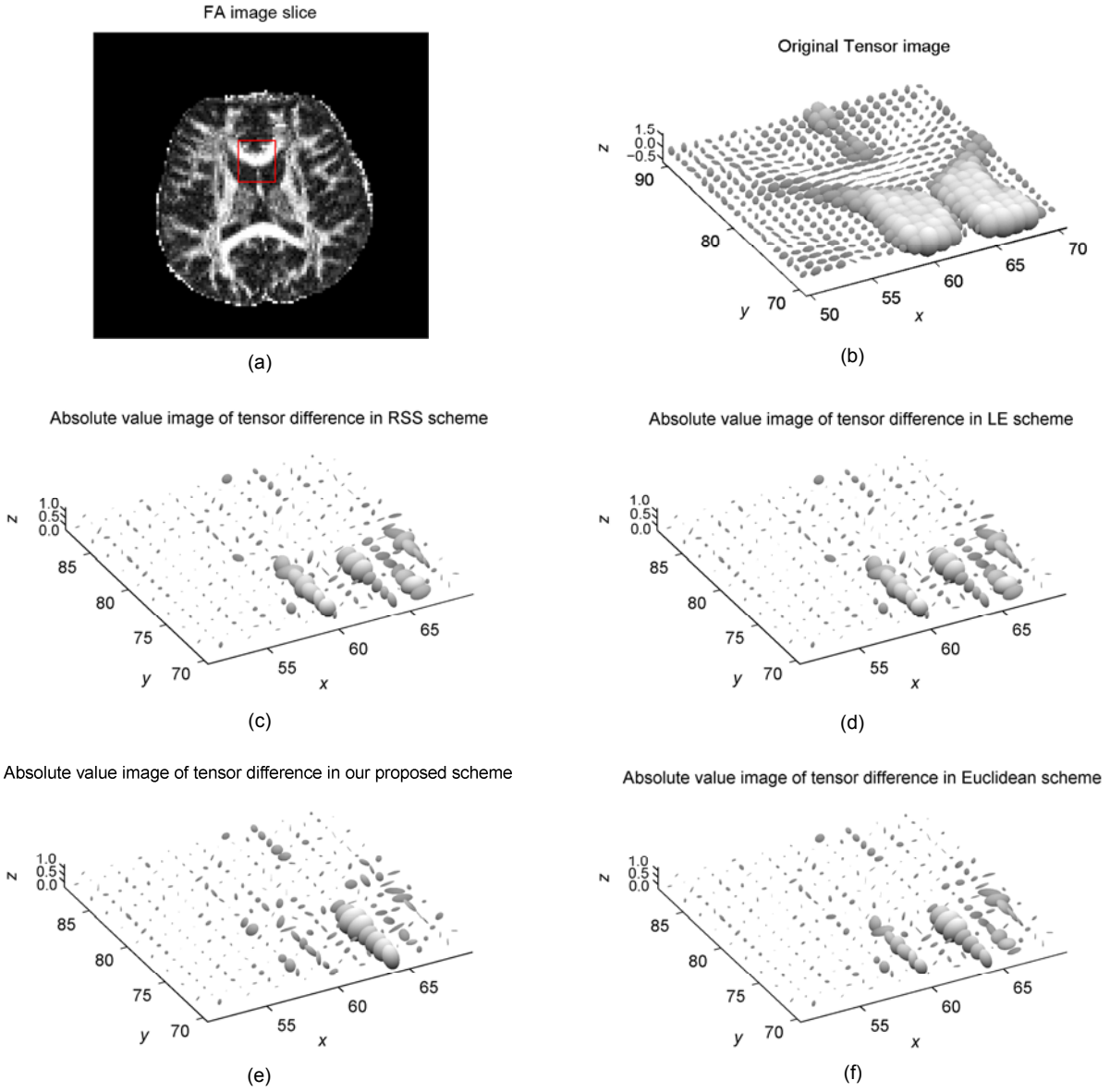

Fig. 4 The fractional anisotropy (FA) image of the selected axial slice (a), the original diffusion tensor ellipsoid image (b), and the reconstruction error ellipsoid images obtained using the RSS scheme (c), the LE scheme (d), our proposed scheme (e), and the Euclidean scheme (f)

The larger ellipsoid represents the larger reconstruction error

proposed scheme has the smallest error. The Euclidean scheme has the smallest error for the Euclidean norm, and the proposed scheme has the smallest error for the Riemannian norm. The elements of the DT matrix in general have the magnitude of 10^{-9} or lower, so the measured values are very small, except for the Riemannian norm, using logarithmic operation.

Table 1 Quantitative comparison between different interpolation schemes

Scheme	Determinant error ($\times10^{-26}$)	Euclidean norm ($\times10^{-7}$)	Riemannian norm ($\times10^{4}$)
Ours	**2.2564**	1.3939	**1.0189**
RSS	3.4339	1.4221	1.0221
LE	3.4355	1.4198	1.0223
Euclidean	2.4127	**1.3580**	1.0232

4 Discussions

4.1 Interpolation profile control

The proposed scheme can control the DT interpolation profile of the determinant using Eqs. (4) and (5) for two tensors and Eqs. (7)–(9) for the DT image. Once a required profile was selected, this scheme was able to control the interpolation according to the profile (Figs. 2 and 3). Using this scheme, it was possible to generate an arbitrary monotonic interpolation profile.

4.2 Reconstruction error for human DTI

4.2.1 Visual observation

In the reconstruction error images of the RSS, LE, the linear profile, and the Euclidean interpolation scheme, the large error ellipsoids occurred within the ventricle. The places where the large error ellipsoids occurred were different for each interpolation scheme. The proposed (linear profile) scheme (Fig. 4e) had the larger error ellipsoids on the x=64 column between left and right ventricles, compared with other schemes. Euclidean (Fig. 4f), RSS (Fig. 4c), and LE (Fig. 4d) schemes had the larger error ellipsoids on the x=60, 66, and 68 columns than the linear profile scheme. Two Riemannian schemes had almost the same error image of diffusion ellipsoids, but were not completely the same.

4.2.2 Quantitative comparison

As shown in Table 1, the linear profile scheme had the smallest determinant error 2.2564×10^{-26}. As we know, the tensor determinant is proportional to the diffusion ellipsoid volume. Thus, this result showed that the linear profile interpolation gave the best reconstruction of the original diffusion volume. As for the Euclidean norm, the Euclidean scheme had the smallest error 1.3580×10^{-7} (Table 1), which can be understood because the Euclidean distance was minimized just due to Euclidean interpolation. For the Riemannian norm, the proposed scheme also had the smallest error, and the Euclidean scheme had the largest error.

Consequently, the proposed linear profile scheme worked better than other schemes. We could explain this as follows: The large errors occurred in the interface between the brain tissues with different diffusibilities (Fig. 4) and the error level depended on the transition pattern on the interface rather than the interpolation scheme. If the transition pattern fitted the linear profile, the reconstruction error was the smallest when using the linear profile scheme as in the x=60 column in Fig. 4e, and if the transition pattern fitted the power function profile, then the error would be the smallest when using the RSS or LE scheme, as in the x=64 column in Figs. 4c and 4d. The experiment results gave two hints: first, perhaps the general configuration of water molecule diffusion in the selected DTI slice is approximate to the linear profile; second, it is necessary to use adaptive interpolation, depending on a local diffusion configuration, to improve the interpolation quality.

5 Conclusions

The proposed scheme uses the non-uniform motion on a Riemannian geodesic to generate a required interpolation profile and preserve the diffusion properties. The reconstruction experiment with an interpolation operation was performed on a human DT image. Here the sites with large reconstruction errors depended on the interpolation schemes. Experimental results showed that the adaptive interpolation was necessary to improve the reconstruction quality. In this work, we resolved the interpolation profile control as a problem for adaptive interpolation. In further work, we will study the methodology to collect the local diffusion pattern information.

Acknowledgements

The authors thank Mr. Biao JIANG with the 2nd Affiliated Hospital, School of Medicine, Zhejiang University, for providing the experimental images.

References

Alexander, D.C., Barker, G.J., 2005. Optimal imaging parameters for fiber-orientation estimation in diffusion MRI. *NeuroImage*, **27**(2):357-367. [doi:10.1016/j.neuroimage.2005.04.008]

Alexander, D.C., Pierpaoli, C., Basser, P.J., Gee, J.C., 2001. Spatial transformations of diffusion tensor MR images. *IEEE Trans. Med. Imag.*, **20**(11):1131-1139. [doi:10.1109/42.963816]

Arsigny, V., Fillard, P., Pennec, X., Ayache, N., 2006. Log-Euclidean metrics for fast and simple calculus on diffusion tensors. *Magn. Reson. Med.*, **56**(2):411-421. [doi:10.1002/mrm.20965]

Bansal, R., Staib, L.H., Xu, D.R., Laine, A.F., Royal, J., Peterson, B.S., 2008. Using perturbation theory to compute the morphological similarity of diffusion tensors. *IEEE Trans. Med. Imag.*, **27**(5):589-607. [doi:10.1109/TMI.2007.912391]

Basser, P.J., Mattiello, J., Bihan, D.L., 1994. MR diffusion tensor spectroscopy and imaging. *Biophys. J.*, **66**(1):259-267. [doi:10.1016/S0006-3495(94)80775-1]

Batchelor, P.G., Moakher, M., Atkinson, D., Calamante, F., Connelly, A., 2005. A rigorous framework for diffusion tensor calculus. *Magn. Reson. Med.*, **53**(1):221-225. [doi:10.1002/mrm.20334]

Chefd'Hotel, C., Tschumperlé, D., Deriche, R., Faugeras, O., 2004. Regularizing flows for constrained matrix-valued images. *J. Math. Imag. Vis.*, **20**(1-2):147-162. [doi:10.1023/B:JMIV.0000011920.58935.9c]

Filley, C.M., 2001. The Behavioral Neurology of White Matter. Oxford University Press, New York, p.299.

Fletcher, P.T., Sarang, J., 2007. Riemannian geometry for the statistical analysis of diffusion tensor data. *Signal Process.*, **87**(2):250-262. [doi:10.1016/j.sigpro.2005.12.018]

Hoptman, M.J., Nierenberg, J., Bertisch, H.C., Catalano, D., Ardekani, B.A., Branch, C.A., DeLisi, L.E., 2008. A DTI study of white matter microstructure in individuals at high genetic risk for schizophrenia. *Schizophr. Res.*, **106**(2-3):115-124. [doi:10.1016/j.schres.2008.07.023]

Jones, D.K., Simmons, A., Williams, S.C.R., Horsfield, M.A., 1999. Non-invasive assessment of axonal fibre connectivity in the human brain via diffusion tensor MRI. *Magn. Reson. Med.*, **42**(1):37-41. [doi:10.1002/(SICI)1522-2594(199907)42:1<37::AID-MRM7>3.0.CO;2-O]

Kindlmann, G., Estépar, R.S.J., Niethammer, M., Haker, S., Westin, C.F., 2007. Geodesic-loxodromes for diffusion tensor interpolation and difference measurement. *LNCS*, **4791**:1-9. [doi:10.1007/978-3-540-75757-3_1]

Pajevic, S., Basser, P.J., 2003. Parametric and non-parametric statistical analysis of DT-MRI. *J. Magn. Reson.*, **161**(1):1-14. [doi:10.1016/S1090-7807(02)00178-7]

Peng, H., Orlichenkob, A., Dawe, R.J., Agam, G., Zhang, S., Arfanakis, K., 2009. Development of a human brain diffusion tensor template. *NeuroImage*, **46**(4):967-980. [doi:10.1016/j.neuroimage.2009.03.046]

Pennec, X., Fillard, P., Ayache, N., 2006. A Riemannian framework for tensor computing. *Int. J. Comput. Vis.*, **66**(1):41-66. [doi:10.1007/s11263-005-3222-z]

Roosendaal, S.D., Geurts, J.J.G., Vrenken, H., Hulst, H.E., Cover, K.S., 2009. Regional DTI differences in multiple sclerosis patients. *NeuroImage*, **44**(4):1397-1403. [doi:10.1016/j.neuroimage.2008.10.026]

Schonberg, T., Pianka, P., Hendler, T., Pasternak, O., Assaf, Y., 2006. Characterization of displaced white matter by brain tumors using combined DTI and fMRI. *NeuroImage*, **30**(4):1100-1111. [doi:10.1016/j.neuroimage.2005.11.015]

Snook, L., Plewes, C., Beaulieu, C., 2007. Voxel based versus region of interest analysis in diffusion tensor imaging of neurodevelopment. *NeuroImage*, **34**(1):243-252. [doi:10.1016/j.neuroimage.2006.07.021]

Stejskal, E.O., Tanner, J.E., 1965. Spin diffusion measurements: spin echoes in the presence of a time-dependent field gradient. *J. Chem. Phys.*, **42**(1):288-292. [doi:10.1063/1.1695690]

Zhang, H., Yushkevich, P.A., Alexander, D.C., Gee, J.C., 2006. Deformable registration of diffusion tensor MR images with explicit orientation optimization. *Med. Image Anal.*, **10**(5):764-785. [doi:10.1016/j.media.2006.06.004]

Zhou, Y.X., Dougherty, J.H., Hubner, K.F., Bai, B., Cannon, R.L., Hutson, R.K., 2008. Abnormal connectivity in the posterior cingulate and hippocampus in early Alzheimer's disease and mild cognitive impairment. *Alzheim. Dement.*, **4**(4):265-270. [doi:10.1016/j.jalz.2008.04.006]

Appendix: Three error measures

1. Determinant error of the absolute value image:

$$V=\sum_{x,y\in\Omega}\det|\boldsymbol{D}_1(x,y)-\boldsymbol{D}_2(x,y)|,$$

where $\boldsymbol{D}_1$ and $\boldsymbol{D}_2$ are the different DT images, Ω is the image range, and $|\cdot|$ represents the absolute value of the difference between corresponding diffusion tensors in $\boldsymbol{D}_1$ and $\boldsymbol{D}_2$. The absolute value of a non-positive definite tensor is obtained by reversing the sign of the negative eigenvalue and then re-computing the tensor (Bansal *et al.*, 2008). Therefore, $\boldsymbol{D}=|\boldsymbol{D}_1-\boldsymbol{D}_2|$ is just the absolute image of the difference of $\boldsymbol{D}_1$ and $\boldsymbol{D}_2$.

2. Euclidean norm of the absolute value image:

$$N_{\mathrm{Eu}}=\sum_{x,y\in\Omega}\sqrt{\mathrm{tr}\,|\boldsymbol{D}_1(x,y)-\boldsymbol{D}_2(x,y)|^2}.$$

3. Riemannian norm (LE norm) of the absolute value image:

$$N_{\mathrm{Ri}}=\sum_{x,y\in\Omega}\sqrt{\mathrm{tr}\,(\log|\boldsymbol{D}_1(x,y)-\boldsymbol{D}_2(x,y)|)^2}.$$